Inductive and Electrostatic Acceleration in Relativistic Jet-Plasma Interactions

Johnny S. T. Ng and Robert J. Noble

Stanford Linear Accelerator Center, Stanford University, Stanford, CA 94309

We report on the observation of rapid particle acceleration in numerical simulations of relativistic jet-plasma interactions and discuss the underlying mechanisms. The dynamics of a charge-neutral, narrow, electron-positron jet propagating through an unmagnetized electron-ion plasma was investigated using a three-dimensional, electromagnetic, particle-in-cell computer code. The interaction excited magnetic filamentation as well as electrostatic plasma instabilities. In some cases, the longitudinal electric fields generated inductively and electrostatically reached the cold plasma wave-breaking limit, and the longitudinal momentum of about half the positrons increased by 50% with a maximum gain exceeding a factor of two during the simulation period. Particle acceleration via these mechanisms occurred when the criteria for Weibel instability were satisfied.

PACS numbers: 98.70.Sa, 98.54.Cm, 52.27.Ny, 52.35.Qz

Relativistic outflows are commonly associated with astrophysical sources such as active galactic nuclei and gamma-ray bursts. Their interaction with ambient plasma is believed to give rise to particle acceleration producing the observed radiation spectrum ranging from radio to gamma-ray. Acceleration occurs when the energy carried by the outflow is transferred to the surrounding material. The subject is an area of active research and has been reviewed elsewhere [1, 2]. In some models, the mechanism relies on the stochastic scattering of particles among the magnetic fields created by magnetohydrodynamic shocks [3]. Alternatively, kinetic energy of the outflow could be converted into plasma instabilities which in turn power particle acceleration and nonthermal radiation [4, 5].

In this Letter, we report on the observation of particle acceleration in simulation studies of relativistic jet-plasma interactions, and elucidate the relevant physical mechanisms. We study the evolution of a narrow, charge-neutral, electron-positron jet propagating through a stationary, unmagnetized electron-ion plasma. This geometry allows us to explore the physics occurring on the plasma wavelength scale both in the jet interior and at the jet-plasma boundary, in the limit of no background magnetic field. Our work sheds light on fundamental questions regarding the processes by which jet-plasma interactions cause particle acceleration.

When charge-neutral plasmas stream through each other it is well-known that filamentation occurs via a process

commonly referred to as the transverse Weibel instability [6, 7]. Essentially, the Lorentz force associated with magnetic field perturbations due to local current imbalances causes the moving neutral plasma to charge-separate transversely, and the resulting current filaments strengthen the azimuthal magnetic field perturbation in a positive feed-back mechanism. The result is that a neutral jet quickly breaks up into oppositely charged filaments. This instability has been suggested as a mechanism for generating strong magnetic fields in the relativistic outflows of active galactic nuclei and gamma-ray bursts [8, 9].

Particle-in-cell (PIC) simulations are well-suited to study these complex phenomenon [10]. Recent PIC simulation studies of filamentation in astrophysical plasmas have concentrated on wide jets using periodic boundary conditions to study the interior dynamics [11, 12, 13, 14]. Astrophysical observations have indicated instabilities might also be taking place at the boundary region of the jet, that is, the interface of the flowing relativistic plasma and surrounding material. It was the goal of this work to simulate the interaction of a narrow relativistic jet where the dynamics in the interior as well as at the jet-plasma boundary can be investigated. We study finite length as well as continuously flowing jets. Our investigation of finite length jets was motivated by the observation of density variations along the length of some astrophysical jets, due to either some type of longitudinal instability or the pulsed nature of the source.

Our PIC code is based on the TRISTAN package modified for our particular problem [15]. TRISTAN is a three-dimensional, electromagnetic, relativistic particle-in-cell code employing a so-called local electromagnetic field solver without the need for transform methods. The temporal and spatial scales are normalized to ω_{pe}^{-1} and $\lambda\!\!\!^{-}_{p}$, respectively, of the background plasma, where $\omega_{pe} = \sqrt{4\pi e^2 n_e/m_e}$ is the electron plasma frequency, and $\lambda\!\!\!^{-}_{p} = \mathrm{c}/\omega_{pe}$ is the collisionless skin depth, c being the speed of light, e the electron charge, n_e the plasma electron density, and m_e the electron mass. The electromagnetic fields are normalized to the cold plasma-wave breaking value $E_{pw} = m_e\, c\, \omega_{pe}/e$. Each simulation run thus represents a family of cases with arbitrary background plasma density because this parameter has been scaled out. The jet's relativistic factor γ, diameter D, length L, and the jet to plasma density ratio α, as well as the time-step size and the number of macro-particles per cell can all be set independently.

Simulations were performed on a $150 \times 150 \times 225$ grid with a total of about 40 million macro-particles. In units of $\lambda\!\!\!^{-}_{p}$, the box size was 30×30 transversely ($x \times y$) and 45 longitudinally (in z). The TRISTAN boundary conditions were set such that radiation at the box walls was absorbed to simulate free space with no reflections. Particles leaving the box were lost from the simulation, although we recorded the energy they carried away. Typically the simulation box was made large enough so that few jet particles ever leave during the entire simulation and less than 0.5% of the

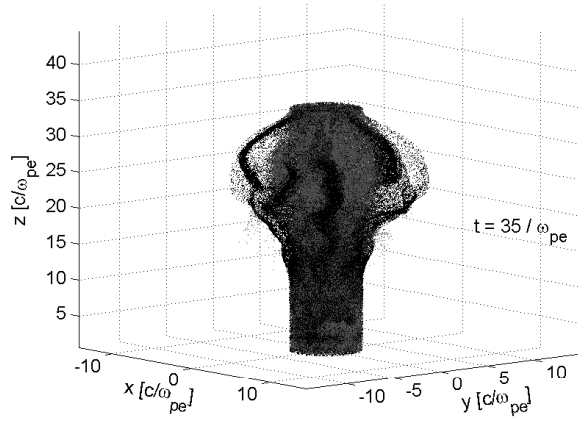

FIG. 1: Spatial distribution of electrons (gray dots) and positrons (black dots) of a continuous jet. The stationary background plasma is not shown.

jet energy was carried away. We varied our simulation parameters, and found that our results were not sensitive to the box size, nor the number of macro-particles per cell once this number was in the range of 4 to 8.

Figure 1 illustrates our simulation geometry and shows a continuous jet of uniform cross-section at a simulation time step of $t = 35\ \omega_{pe}^{-1}$. The stationary electron-ion plasma fills the entire box uniformly and defines the laboratory frame where physical parameters are given. The jet enters at the bottom of the simulation box and travels along the z direction. To discuss a concrete example in the following, we choose the jet parameters to be $\gamma = 10$, $\alpha = 10$, $D = 6\ \lambda_p$, $L = 10\ \lambda_p$, and the RMS transverse velocity spread $\Delta v_\perp/c = \Delta\beta_\perp = 10^{-4}$. Estimates of the physical parameters for astrophysical outflows span many orders of magnitude. The dimensions of jets we can simulate are much smaller than those in astrophysical environments, but the dynamics of interest here occur on the scale of a plasma wavelength. The plasma physics in this example occur within a duration of $45\ \omega_{pe}^{-1}$. A time-step size of $0.1\ \omega_{pe}^{-1}$ was adequate to resolve this physics, as confirmed by runs with $0.05\ \omega_{pe}^{-1}$ time-steps. For a Courant parameter of 0.5, this corresponded to a mesh size of $0.2\ \lambda_p$. We have performed simulations with a range of parameters: $\alpha = 0.1$ to 100, $\Delta\beta_\perp = 10^{-4}$ to 10^{-1}, $D = 6$ to $60\ \lambda_p$, and $\gamma = 10$ to 100. We give a summary of our parameter variation studies at the end.

The fundamental issue here is how jet-plasma instabilities can lead to particle acceleration. In our simulations, we observe the Weibel instability as the first step in this process. The electromagnetic energy grows exponentially and then saturates, and eventually dissipates. The growth rate in the laboratory frame is approximately $\omega_{pj}/\sqrt{\gamma}$ [16], where $\omega_{pj} = \sqrt{4\pi e^2 n_j/m_e}$ is the jet's plasma frequency, n_j being the jet density. The jet filament size is on the order

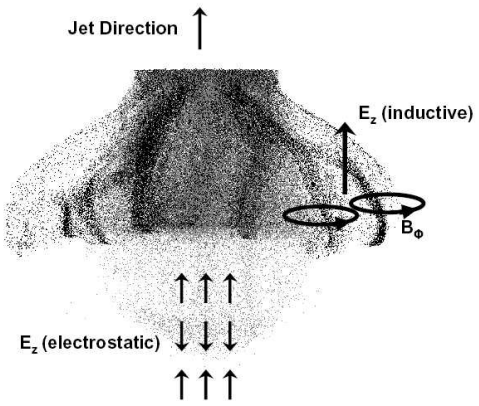

FIG. 2: Side view of a 10 λ_p long, 6 λ_p wide jet at simulation time $t = 35\ \omega_{pe}^{-1}$, showing positron filaments (black dots) expelled from the jet leaving behind the electrons (gray dots). It also illustrates the mechanisms for generating inductive as well as electrostatic longitudinal electric fields.

of c/ω_{pj}. Our simulations confirm the scaling with n_j and γ. The instability saturates at approximately 10% of the initial jet energy at $t = 20\ \omega_{pe}^{-1}$, and dissipates to about 65% of the maximum value by $t = 45\ \omega_{pe}^{-1}$.

As the jet continues to plow forward, the Lorentz force between the electron and positron filaments tend to push them apart. The electron filaments, however, are confined by the electrostatic channel formed by the heavier-mass background plasma ions ($m_i = 192\, m_e$). The positron filaments are preferentially expelled from the interior of the jet. The filaments near the surface escape first, followed by the interior ones as they sequentially migrate outward. As the positron filaments move away from the interior and from each other, the azimuthal magnetic field (B_ϕ) associated with the filaments decreases rapidly. According to Faraday's law of induction, the time-variation of magnetic flux generates a loop-integrated electric field enclosing the flux region. In our simulation, we find that this large and negative $\dot{B}_\phi$ locally induces a large and positive longitudinal electric field E_z, as illustrated in Figure 2. Furthermore, once separated, these charged filaments also generate longitudinal electrostatic oscillations in the background plasma.

These two types of longitudinal electric fields in our simulations are represented by the two dominant features shown in Figure 3. The inductive nature of the fields is demonstrated by the anti-correlation between E_z and $\dot{B}_\phi$ in the upper-left quadrant of the plot. The electrostatic component corresponds to the cluster of points near $\dot{B}_\phi = 0$, with both positive and negative polarities. The waveforms of these fields are shown explicitly in Figure 4 at three epochs during the simulation.

The inductively generated E_z field propagates at the same relativistic velocity as the filaments, and persists through-

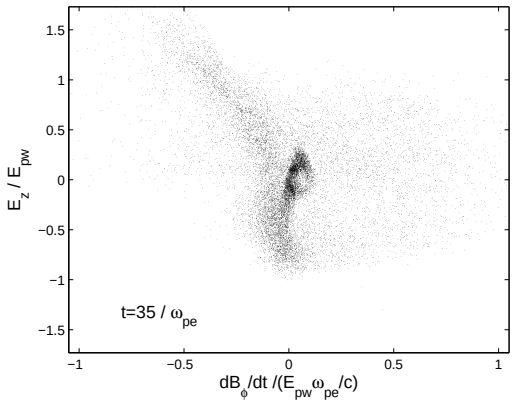

FIG. 3: Correlation of longitudinal electric field with time variation of azimuthal magnetic field at the same spatial location for a 10 λ_p long, 6 λ_p wide jet. For clarity, only a random subset of field points outside a radius of 2.5 λ_p are shown.

out the simulation duration. Based on experience with terrestrial accelerators, this E_z can efficiently accelerate particles as they "surf" on a wave of electric fields in the direction of motion. In this case, it preferentially accelerates comoving positrons and decelerates electrons.

As the charge filaments separate, we found that starting at about 25 ω_{pe}^{-1}, a coherent train of longitudinal plasma oscillations was excited behind the jet analogous to the wake of a ship in water. They have no associated transverse magnetic field over their interior volume, and only limited surface magnetic fields at their extreme edges, as expected for finite-size plasma waves. These plasma wakefields have a phase velocity equal to the speed of the drive jet, and have amplitudes of order the wave-breaking limit for the parameters of this simulation. Plasma wakes always form immediately behind the trailing edge of the jet, regardless of its length. They continue to oscillate after the drive jet passes, and hence can accelerate relativistic particles over very long distances [5, 17].

The longitudinal momentum (p_z) distributions of jet positrons and electrons are shown in Figure 5. On average the positrons gained energy, with approximately half of the initial population increasing at least 50% in p_z. The electrons generally lost energy during the process. The positron energy change of about 15 $m_e c^2$ during the simulation is consistent with acceleration over a distance of 10 to 20 λ_p by a longitudinal electric field of order E_{pw} (which can also be written as $m_e c^2/e\lambda_p$.) The transverse momentum of the jet particles broadened significantly from the initial distribution. Some of the initial jet energy was also converted into heating the background plasma, with the thermal energy of plasma electrons increased to approximately $m_e c^2$.

To explore the generality of our results, we varied the physical parameters in our simulations as described earlier.

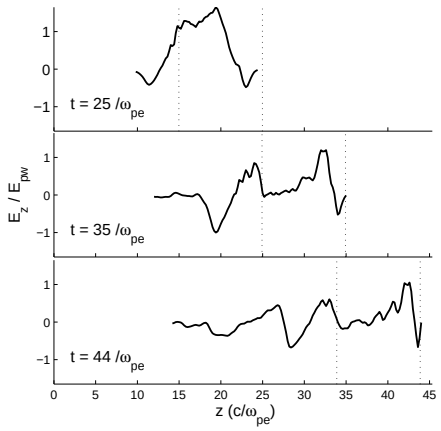

FIG. 4: Longitudinal electric field as a function of z at a given point $(x, y) = (2.25, 1.25)\ \lambda_p$. The dotted lines bracket the 10 λ_p long jet. Note the predominantly inductive E_z at $t = 25\ \omega_{pe}^{-1}$, and the wakefield left behind the jet at later times.

We observe inductive and wakefield acceleration for the parameter regime where the Weibel instability occurs. Both continuous and finite-length jets exhibit the same transverse (Weibel) dynamics but different longitudinal dynamics. The longitudinal electrostatic fields are much stronger in the finite-length case. Varying the jet diameter does not affect the acceleration mechanisms that we observe. As the jet diameter is increased, we observe the same expulsion of positron filaments from the surface as in the narrower jet case, as well as the interior filaments of the same sign coalescing within the jet.

For a finite length jet, the maximum E_z is approximately proportional to α for $\alpha < 1$. This linear behavior has been observed in previous studies of plasma wakefield accelerators [17]. For $\alpha > 1$, the scaling we observe is approximately $\alpha^{0.5}$. We also observe almost complete expulsion of the background plasma electrons by the jet and formation of a focusing ion channel. This case is similar to the so-called "blow-out" regime previously studied in electron beam-plasma interactions [17, 18].

The density ratio and jet temperature are expected to affect the dynamics of the Weibel instability [16]. For a given density ratio, increased temperature provides a pressure that opposes the transverse magnetic pinching force. The threshold condition for instability is approximately $\alpha > \gamma(\Delta\beta_\perp)^2$ for a relativistic jet. This threshold condition was satisfied over nearly the entire range of our simulation parameters. The range of $\Delta\beta_\perp$ in our study is similar to those of earlier studies of Weibel instability in astrophysical plasmas [11, 12, 13, 14]. To test the instability criteria, we simulated a case with $\alpha = 0.1$ and $\Delta\beta_\perp$ approximately equal to 0.1 for $\gamma = 10$. No Weibel instability was observed

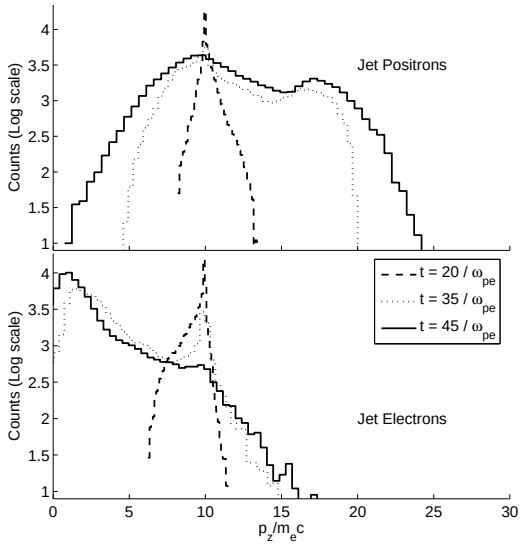

FIG. 5: Longitudinal momentum distribution of jet positrons and electrons at three simulation epochs for a 10 λ_p long jet, showing positron acceleration and electron deceleration.

over a period of 180 ω_{pe}^{-1}. The implication is that for hot, tenuous jets, Weibel filamentation is suppressed.

The Weibel instability is believed to occur in astrophysical environments where relativistic outflows exist [8, 9, 11, 12, 13, 14]. Our results indicate that when the Weibel instability occurs, an inductive "Faraday acceleration" mechanism can effectively power cosmic particles, and electrostatic plasma wakefields are excited by an initially charge-neutral jet when oppositely charged filaments separate. We expect the longitudinal electric fields observed in our simulation will continue to be generated as the jet propagates over long distances. Relativistic particles will be accelerated as long as they remain in phase with these waves. Due to the velocity difference, acceleration occurs for at most one half period of phase slip between the particle at velocity c and the slower wave at $0.995c$ created by the $\gamma = 10$ jet. The dephasing length is approximately $\gamma^2\lambda_p = 200\pi\lambda_p$, and thus the energy gain is about 300 MeV for an accelerating field of order E_{pw}. This is a plausible mechanism for creating a population of relativistic particles that give rise to the observed gamma-rays. It could also serve as the first stage injection mechanism for other ultra-high energy cosmic ray acceleration models.

These simulations have implications for future research. The jet-plasma interaction should be followed for a much longer time to study the effect of particle acceleration over long distances. The effect of background magnetic fields should be investigated, as well as different particle mixtures of jet and background plasma compositions. Synchrotron radiation can be readily implemented in a particle-in-cell code and the resulting spectrum can be verified against ob-

servation. Advances in accelerator technology will enable jet-plasma dynamics to be studied in a terrestrial laboratory environment [19]. Experimental results will provide important tests of simulations, thus improving the connection between simulations and observations. The work presented here provides the basis for these experiments.

We appreciate discussions with K.-I. Nishikawa, K. Reil, A. Spitkovsky, and M. Watson. We would also like to thank P. Chen, R. Ruth, and R. Siemann for their support and encouragement. Work supported by the U.S. Department of Energy under contract number DE-AC02-76SF00515.

[1] R. D. Blandford, Astrophys. J. Supp. Ser. **90**, 515 (1994).

[2] J. G. Kirk, in *Proc.* 22^{nd} *Texas Symp. on Rel. Astrophys.*, edited by P. Chen *et al.* (2005), SLAC-R-752.

[3] J. G. Kirk and P. Duffy, J. Phys. G **25**, 163 (1999), for a review.

[4] R. Schlickeiser *et al.*, Astroph. and Astron. **393**, 69 (2002).

[5] P. Chen, T. Tajima, and Y. Takahashi, Phys. Rev. Lett. **89**, 161101 (2002).

[6] E. S. Weibel, Phys. Rev. Lett. **2**, 83 (1959).

[7] P. H. Yoon and R. C. Davidson, Phys. Rev. A **35**, 2718 (1987).

[8] M. V. Medvedev and A. Loeb, Astroph. J. **526**, 697 (1999).

[9] M. V. Medvedev *et al.*, Astroph. J. **618**, L75 (2005).

[10] C. K. Birdsall and A. B. Langdon, *Plasma Physics via Computer Simulation* (IOP Publishing Ltd., Bristol, England, 1991).

[11] L. O. Silva *et al.*, Astrophys. J. **596**, L121 (2003).

[12] J. T. Frederiksen *et al.*, Astrophys. J. **608**, L13 (2004).

[13] C. B. Hededal *et al.*, Astrophys. J. **617**, L107 (2004).

[14] K. I. Nishikawa *et al.*, Astrophys. J. **622**, 927 (2005).

[15] O. Buneman, in *Computer Space Plasma Physics: Simulation Techniques and Software*, edited by H. Matsumoto and Y. Omura (Terra Scientific Publishing, Tokyo, Japan, 1993).

[16] L. O. Silva *et al.*, Phys. Plasmas **9**, 2458 (2002).

[17] E. Esarey *et al.*, IEEE Trans. Plasma Science **24**, 252 (1996), for a review.

[18] S. Lee *et al.*, Phys. Rev. E. **61**, 7014 (2000).

[19] J. S. T. Ng, in *Proc.* 28^{th} *ICFA Advanced Beam Dynamics Workshop* (Higashi Hiroshima, Japan, 2003), SLAC-PUB-10134.